



Effect of weld penetration on low-cycle fatigue strength of load-carrying cruciform joints

Takeshi Hanji¹ · Kazuo Tateishi¹ · Yuko Ohashi¹ · Masaru Shimizu¹

Received: 2 September 2018 / Accepted: 25 November 2019 / Published online: 13 December 2019
© International Institute of Welding 2019

Abstract

This study examined the low-cycle fatigue behavior of load-carrying cruciform-welded joints containing incomplete penetration. Five types of specimens with different sizes of weld penetrations and weld leg lengths were tested under cyclic plastic strains. During testing, cracking behavior was observed on the side surface of the specimen. The test results revealed that the fatigue strength and cracking patterns depend on the ratio of the weld penetration to the main plate thickness and the ratio of the weld leg length to the main plate thickness, respectively. Elasto-plastic finite element analyses including the effective notch concept were then performed. The results indicate that the fatigue strength and cracking pattern of the specimens can be correlated with the local strain distribution around the effective notch.

Keywords Low-cycle fatigue · Load-carrying cruciform-welded joints · Weld penetration · Local strain

1 Introduction

Defects and imperfections in welds, which are often detected in steel members, have a negative effect on the fatigue strength of welded joints. For example, internal flaws such as incomplete penetration are often reported at beam-to-column connections of steel bridge bents, which are widely used in elevated highways in urban areas [1] and at connections in seismic resisting systems to prevent bridges from collapse during a huge earthquake, although they are designed to be fabricated with full-penetration welds.

When large cyclic plastic strains due to excessive external force, such as those due to an earthquake, are induced in welded joints with defects and imperfections, the joints may develop a higher risk of low-cycle fatigue failure because of strain concentrations newly generated by the defect. In particular, incomplete penetration is a crack-like notch and can easily trigger fatigue cracking due to high strain concentration.

Therefore, the effect of weld defects on the low-cycle fatigue strength of welded joints should be carefully investigated.

Extensive research on the fatigue performance of welded joints containing incomplete penetration has been conducted in high-cycle fatigue regions [2–8]. It has been demonstrated that the fatigue life of load-carrying cruciform-welded joints with incomplete penetration can be predicted based on a fracture mechanics approach. Moreover, limit curves separating weld toe and root failure in cruciform joints have been developed.

In low-cycle fatigue regions, the effect of weld defects on fatigue performance has been investigated with butt-welded joints [9, 10]. In addition, low-cycle fatigue behavior of cruciform-welded joints has been revealed primarily from the viewpoint of the strength mismatch between the base metal and the weld metal, and a fatigue strength evaluation method based on a local strain approach has been proposed [11–14]. These studies [11–14] focused primarily on a fatigue crack occurring from the weld root and propagating into a weld bead or along a fusion line. On the other hand, in order to establish a method for predicting failure patterns between weld toe and root failures of cruciform joints with incomplete penetration, it is necessary to consider the fatigue strength, including both weld toe and root failures.

In this study, focusing on weld toe failure, the low-cycle fatigue strength and cracking patterns of load-carrying cruciform-welded joints were investigated through experiments and elasto-plastic finite element analyses.

Recommended for publication by Commission XIII - Fatigue of Welded Components and Structures

✉ Takeshi Hanji
hanji@civil.nagoya-u.ac.jp

¹ Nagoya University, Nagoya, Japan

Fig. 1 Specimens (unit:mm). **a** Load-carrying cruciform joint. **b** Detail of welded part. **c** Round bar specimen

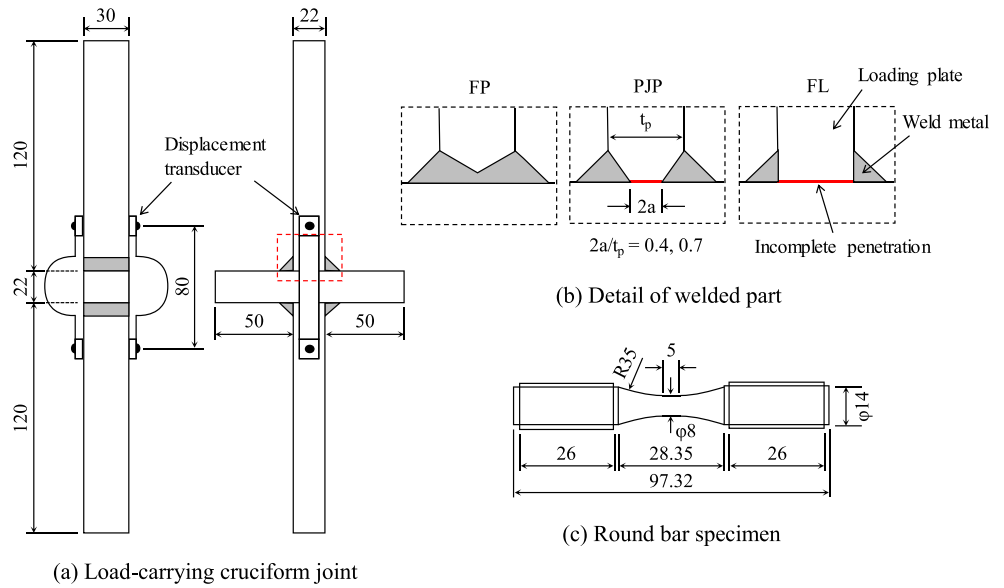


Table 1 Welding conditions

| Welding | Material | Current (A) | Voltage (V) | Welding speed (mm/min) | Heat input (kJ/mm) |
|--|------------------|-------------|-------------|------------------------|--------------------|
| CO ₂ gas-shielded arc welding | JIS Z 3312 YGW11 | 240~270 | 33~35 | 212~514 | 1.04~2.53 |

Fig. 2 Macrographs of specimens. **a** FP **b** PJP40. **c** PJP70. **d** FL. **e** FLH

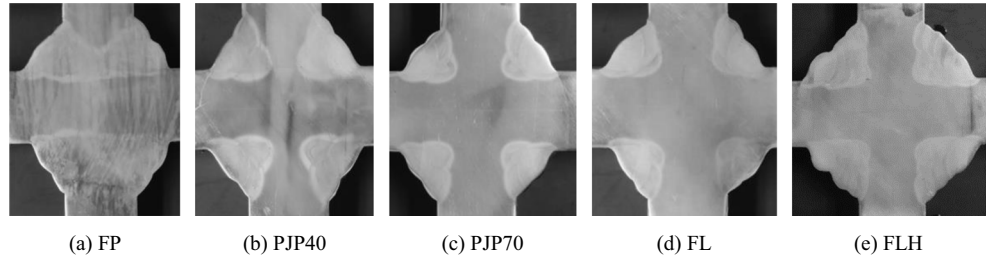
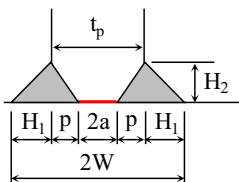


Table 2 Measurement results

| Specimen name | t_p (mm) | $2a$ (mm) | H_1 (mm) | H_2 (mm) | $2W$ (mm) | p (mm) | $2a/t_p$ | a/W | H_1/t_p |
|---------------|------------|-----------|------------|------------|-----------|----------|----------|-------|-----------|
| FP | 22 | 0 | 9.97 | 14.98 | 41.93 | 11.00 | 0 | 0 | 0.45 |
| PJP40 | 22 | 9.73 | 10.98 | 13.27 | 43.97 | 6.13 | 0.44 | 0.22 | 0.50 |
| PJP70 | 22 | 16.02 | 10.53 | 11.15 | 43.07 | 2.99 | 0.73 | 0.37 | 0.48 |
| FL | 22 | 17.70 | 12.70 | 12.27 | 47.40 | 2.15 | 0.80 | 0.37 | 0.58 |
| FLH | 22 | 18.12 | 16.85 | 18.08 | 55.70 | 1.94 | 0.82 | 0.33 | 0.77 |



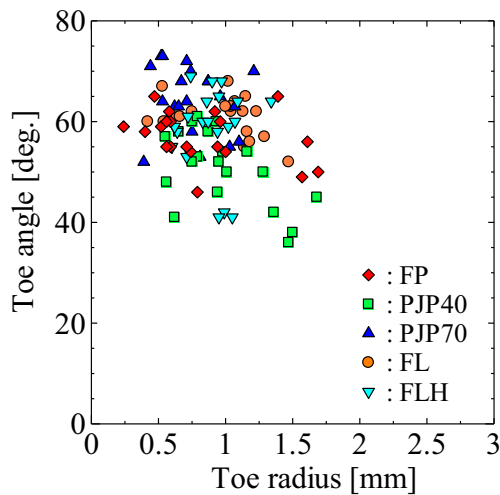


Fig. 3 Weld toe measurement

2 Low-cycle fatigue tests

2.1 Specimen configurations

Low-cycle fatigue tests were performed in load-carrying cruciform-welded joints as shown in Fig. 1. The specimens were made of 22-mm JIS SM400 class steel with various weld penetrations and weld leg lengths. There are three categories of the specimens, which are denoted as FP, PJP, and FL. The FP and FL specimens were fabricated by full-penetration welds and fillet welds, respectively. Partial joint penetration groove welds were applied to the PJP specimens. The PJP specimens were designed to have incomplete penetration ratios of 40% and 70% (denoted as PJP40 and PJP70, respectively). The incomplete penetration ratio is the ratio between the length of unfused portion ($2a$) and the thickness of the loading plate (t_p). The FL specimens were prepared for two sizes of weld leg lengths, where FLH denotes the specimen in which the leg length is larger. Each type has three specimens for fatigue tests and measurements. The weld root gaps were set to be approximately 0 mm. The welding conditions are listed in Table 1. CO₂ gas-shielded arc welding with a solid wire of 1.2 mm in diameter (JIS Z 3312 YGW11) was used to fabricate the specimens. The specimen was fabricated under the condition that the loading plate was placed in the horizontal state during welding.

Table 3 Weld toe measurement results

| Specimen name | Toe radius (mm) | Toe angle (deg) |
|---------------|-----------------|-----------------|
| FP | 0.84 | 57 |
| PJP40 | 0.98 | 51 |
| PJP70 | 0.76 | 64 |
| FL | 0.96 | 61 |
| FLH | 0.89 | 58 |

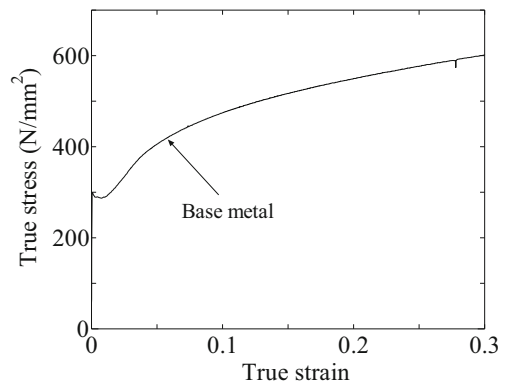


Fig. 4 Tensile test result

Macroetch tests were carried out to locate the weld metal, base metal, and heat-affected zones. Macrographs of the specimen are shown in Fig. 2. The weld leg length (H_1 , H_2), the length of the unfused portion ($2a$), and the weld penetration (p) were measured from photographs, and their average values are given in Table 2. The incomplete penetration ratio ($2a/t_p$) and weld leg length ratio (H_1/t_p) in the specimen ranged from 0 to 0.82 and 0.45 to 0.77, respectively. Based on the limit curve separating the weld toe and root failures in cruciform joints [2, 6], the PJP40, PJP70, FL, and FLH specimens are satisfied by the condition that ensures weld root failure in the high-cycle fatigue region.

Weld bead profiles consisting of the weld toe radius and the toe angle were measured for each specimen. The measurement was performed using a replica method, in which silicon replicas of weld bead were sliced; then, a profile of each sample was measured by image analysis. The number of samples for each type was about 20 on average. The measurements of weld toe configurations are shown in Fig. 3, and their average values are given in Table 3. All of the specimens have similar toe configurations, regardless of specimen type.

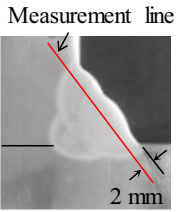
2.2 Mechanical properties of materials

In order to determine the material properties of the base metal (BM), tensile tests were conducted using the round bar specimen shown in Fig. 1. The round bar specimen was cut from the steel plate in the specimen. In the tensile test, the true strain in the loading direction was calculated from the change in the diameter at the throat of the round bar specimen measured by a displacement transducer. The tensile test result is shown in Fig. 4 and Table 4.

Table 4 Mechanical properties

| Material | Yield stress (N/mm ²) | Tensile strength (N/mm ²) |
|-----------------|-----------------------------------|---------------------------------------|
| Base metal (BM) | 299 | 451 |

Table 5 Hardness test results

| | Material | FP (Hv) | PJP40 (Hv) | PJP70 (Hv) | FL (Hv) | FLH (Hv) |
|---|--------------------------|---------|------------|------------|---------|----------|
|  | Base metal (BM) | 167 | 170 | 168 | 169 | 171 |
| | Weld metal (WM) | 199 | 200 | 200 | 201 | 203 |
| | Heat-affected zone (HAZ) | 183 | 197 | 196 | 206 | 211 |

Vickers hardness tests were performed in all types of the specimen, and their average values are given in Table 5. A measurement line is shown in the table. The average values are almost similar between the weld metal (WM) and the heat-affected zone (HAZ), which are approximately 20% higher than that of the base metal (BM). Generally speaking, the strength mismatch between the weld metal and the base metal (WM/BM) implies that a joint with a value of less than 1.0 indicates the occurrence of under-matching and that with a value of more than 1.0 indicates the occurrence of over-matching. Considering the correlation of the hardness and material strength of steel [15], the specimen can be estimated to be approximately 20% over-matched.

2.3 Experimental procedures

Low-cycle fatigue tests were conducted by a fatigue testing machine with an electric hydraulic servo system, the dynamic and static loading capacities are 300 kN and 450 kN, respectively. PI displacement transducers (referred to hereinafter as PI gauge) of 80 mm in gauge length were mounted to both side surfaces of the loading plate over the weld roots, as shown in Fig. 1. During testing, the fluctuation range of the displacement measured by the PI gauge was controlled to be constant. The displacement ranges were 0.8, 1.0, and 1.2 mm.

The minimum displacement was set to be 0 mm. A cyclic load with a low loading rate of 0.05 mm/s was applied to the specimen.

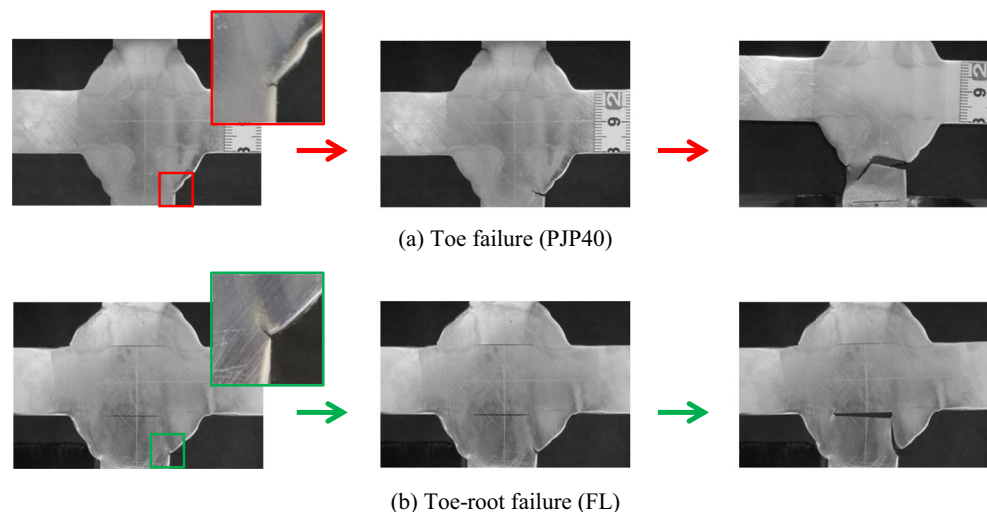
The side surface of the specimen was periodically photographed with a digital camera at the maximum load in loading loops to record the crack initiation and propagation behavior. The PI gauge was removed in order to facilitate crack monitoring, after the relations of the displacement values between the PI gauge and the loading jack became stable, and the displacement range of the jack was then controlled instead of that of the PI gauge. The test was stopped, and the specimen was broken statically after the maximum load was drastically decreased.

3 Experimental results

3.1 Crack initiation and propagation

Figure 5 shows photographs taken at the side surface of the specimen during the test, and the crack lengths measured from the photographs are summarized in Fig. 6. In all of the specimens, a fatigue crack was initiated from a weld toe. After crack initiation, crack propagation patterns differ depending on the incomplete penetration ratio and the weld leg length

Fig. 5 Cracking patterns (displacement range: 0.8 mm). **a** Toe failure (PJP40). **b** Toe-root failure (FL)



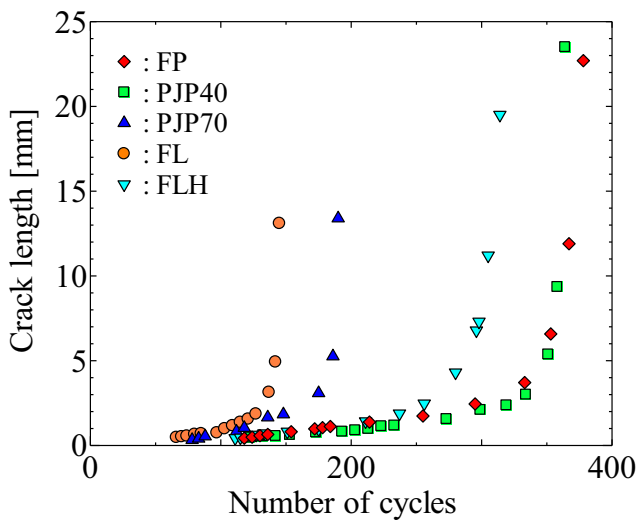


Fig. 6 Crack length vs number of cycles (displacement range: 0.8 mm)

ratio. In the FP, PJP40, and FLH specimens, which have small incomplete penetration ratio or large weld leg length ratio, the crack passed through the loading plate. On the other hand, the crack propagated along a fusion line to a weld root in the PJP70 and FL specimens. In this study, the former is referred to as toe failure, and the latter is referred to as toe-root failure. A crack growing along the fusion line was also observed in a previous study [12], but this crack grew from the weld root.

Figure 7 indicates fracture surfaces of the toe failure and toe-root failure specimens, respectively. A crack grows from the weld toe into the loading plate or along the fusion line to the weld root. No crack was initiated from the weld root in any of the toe-root failure specimens.

3.2 Changes in maximum load

Figure 8 shows the relationship between the change in the maximum load and the number of cycles when the displacement range was 0.8 mm. The ordinate represents the ratio of the maximum load of each cycle to that of the initial cycle. The maximum load decreases with the number of load cycles, although materials used in the specimen generally show cyclic hardening behavior which can be actually observed in a previous study [11] using the materials similar to this study. This decrease in load may be caused by crack occurrence and its

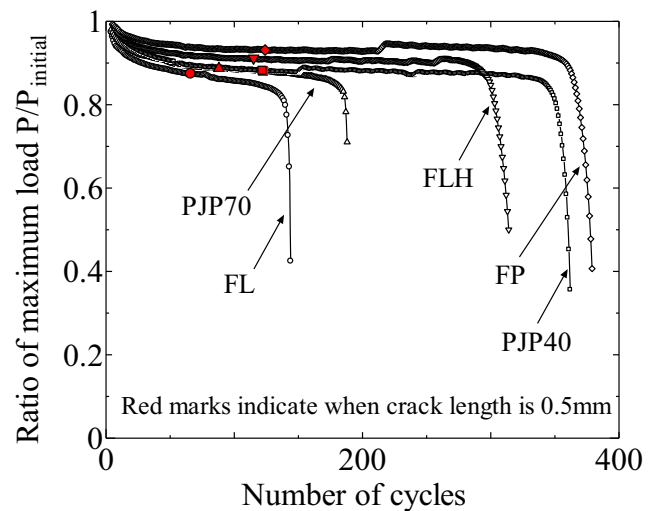


Fig. 8 Changes of maximum load (displacement range: 0.8 mm)

growth with cyclic loading. The red marks in the graph show when the crack length in Fig. 6 reaches 0.5 mm. The maximum load decreases by approximately 10% due to the crack growth to 0.5 mm.

3.3 Fatigue life

The low-cycle fatigue test results are shown in Fig. 9. The ordinate represents the nominal strain range, as calculated by dividing the displacement range applied to the specimen by the gauge length of the PI gauge. The abscissa represents the fatigue life, which is defined as the number of cycles at which the crack length indicated in Fig. 6 reached 0.5 mm. In the graph, the fatigue test results obtained in previous studies [11, 12] are also indicated. The details of the specimens are summarized in Table 6. The tests were conducted using 25% over-matched cruciform joints, and the fatigue cracks from the weld root, referred to hereinafter as root failures, were observed in all specimens. The fatigue life was defined as the number of cycles at which the maximum load decreased by 10% due to crack propagation, which can be considered to be almost equivalent to the fatigue life definition in this study.

The fatigue strength of the specimen is shown to depend on failure pattern, meaning that the toe failure has a higher fatigue strength than the root failure. Among the specimens with a toe

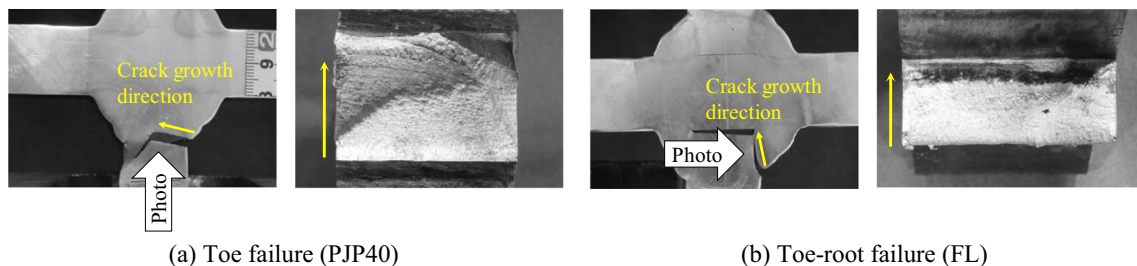


Fig. 7 Fracture surfaces (displacement range: 0.8 mm). a Toe failure (PJP40). b Toe-root failure (FL)

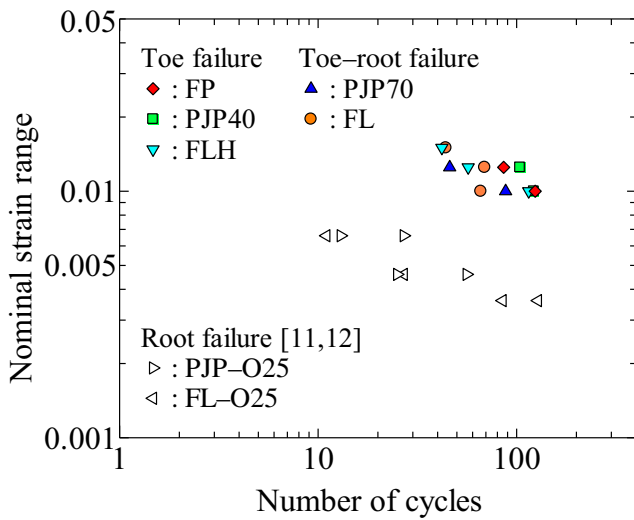


Fig. 9 Fatigue test results

crack, the fatigue strength of the toe-root failure is slightly lower than that of the toe failure.

The test results mentioned above indicated that the fatigue strength and cracking patterns of the load-carrying cruciform-welded joints are influenced by the incomplete penetration ratio and the weld leg length ratio in the low-cycle fatigue region.

4 Finite element analyses

Elasto-plastic finite element analyses were performed in order to investigate the local strain behavior around a cracking point in the specimens of all types.

4.1 Analysis models

Figure 10 shows an example of the FE model and the boundary conditions. Two-dimensional analyses under plane strain assumption were performed with ABAQUS code. A one-quarter symmetry model was created by taking advantage of symmetry.

The measured geometric parameters given in Table 2 were reflected in the model. The concept of a fictitious notch [16] with a radius of 1.0 mm, which is referred to as effective

Table 6 Specimen configuration [11, 12]

| Specimen name | t_p (mm) | $2a/t_p$ | a/W | H_1/t_p | WM/BM |
|---------------|------------|----------|-------|-----------|-------|
| FL-O25 | 28 | 0.86 | 0.52 | 0.32 | 1.27 |
| | 28 | 0.88 | 0.52 | 0.34 | 1.26 |
| PJP-O25 | 28 | 0.62 | 0.43 | 0.22 | 1.27 |
| | 28 | 0.61 | 0.44 | 0.18 | 1.26 |

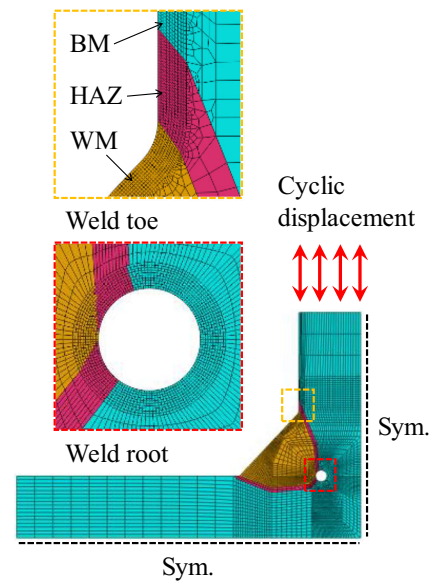


Fig. 10 FE model (PJP70)

notch, was adopted for the weld toe and root. For quantitative comparison among all models, the vicinity of the notch was meshed in the similar configuration. The minimum element size was 0.05 mm [12].

Based on the macrographs shown in Fig. 2, the base metal region (BM), the weld metal region (WM), and the heat-affected zone (HAZ) were individually modeled in the FE mesh. Different stress-strain relationships were assigned to each zone. As for the base metal region, the stress-strain relationship obtained in the tensile test shown in Fig. 4 was used. Based on the results of the hardening test as mentioned above, considering the correlation of the hardness and material strength of steel [15], the weld metal region and the HAZ were assumed to have a 20% higher yield stress than the base metal (BM: 169 Hv, WM: 201 Hv, HAZ: 199 Hv on average). The combined isotropic/kinematic hardening model provided in ABAQUS was applied to all regions. Young’s modulus and Poisson’s ratio were 200 kN/mm² and 0.3, respectively.

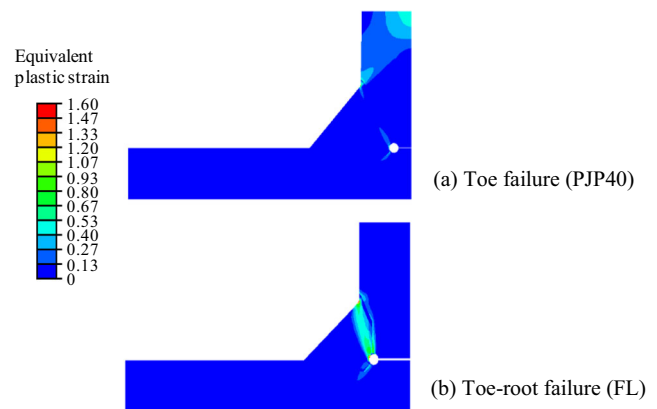


Fig. 11 Strain distributions. a Toe failure (PJP40). b Toe-root failure (FL)

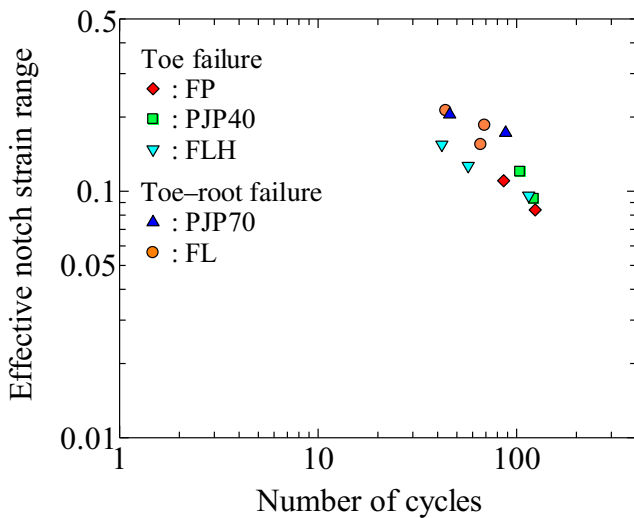


Fig. 12 Fatigue strength evaluation with effective notch strain range

Tensile and compressive loads were applied to the loading plate with displacement control, as in the experiment. In the analysis, crack initiation and propagation were not considered.

4.2 Strain distributions

The equivalent strain distributions after 5.5 loading cycles are shown in Fig. 11. High strains occur from the weld toe to the loading plate in the FP, PJP40, and FLH specimens, which fail due to toe failure. On the other hand, the strain concentration can be observed along the fusion line in the PJP70 and FL specimens that exhibited toe-root failure. The strain distribution agrees with the cracking path in the specimen.

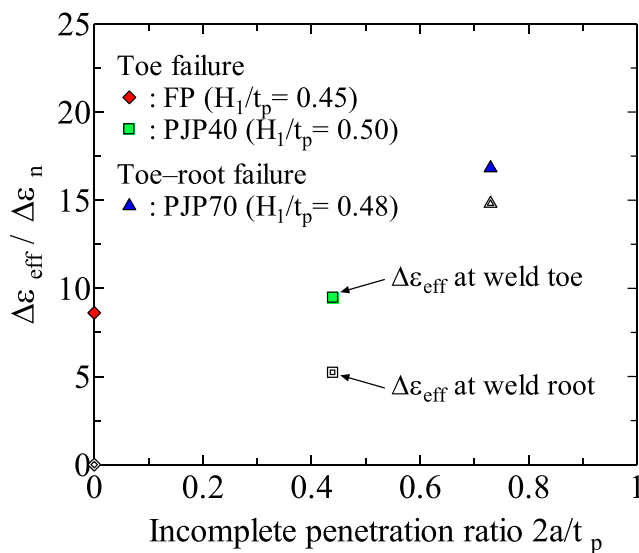


Fig. 13 Effect of incomplete penetration ratio

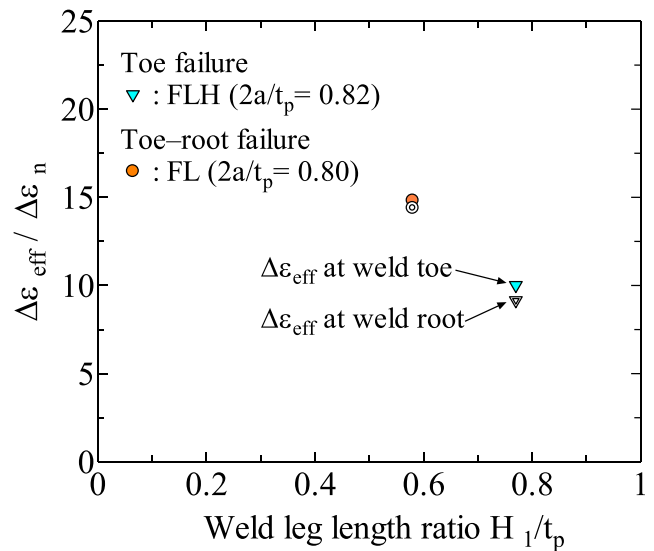


Fig. 14 Effect of weld leg length ratio

4.3 Fatigue strength evaluation using effective notch strain

The maximum value of the equivalent total strain range calculated in the element along the notch is used as the effective notch strain range in this study [12]. Figure 12 shows the relationship between the effective notch strain range and the fatigue life. The effective notch strain range was obtained at the weld toe for the toe and toe-root failure specimens. The differences in the fatigue strength due to specimen type (failure pattern) become small. The effective notch strain can be successfully used to evaluate the fatigue strength of the load-carrying cruciform joints with incomplete penetration, regardless of the incomplete penetration ratio and the weld leg length ratio.

4.4 Indication of cracking points

The effective notch strain range is one of the governing parameters for the low-cycle fatigue strength as mentioned above. Thus, a cracking point was correlated with the effective notch strain value, and the toe, toe-root, and root failure occurrences were investigated.

Table 7 Ratio of effective notch strain range

| Specimen name | Failure pattern | Average of $\Delta\epsilon_{eff,root}/\Delta\epsilon_{eff,toe}$ |
|---------------|-----------------|---|
| FP | Toe | 0 |
| PJP40 | Toe | 0.55 |
| PJP70 | Toe-root | 0.88 |
| FL | Toe-root | 0.97 |
| FLH | Toe | 0.92 |
| Ref. [14] | Root | 1.18–1.33 |

Figure 13 shows the effective notch strain range in terms of the incomplete penetration ratio among the FP, PJP40, and PJP70 specimens, in which the weld leg length ratio is almost same. The ordinate represents the effective notch strain range at the weld toe and root ($\Delta\varepsilon_{\text{eff,toe}}$, $\Delta\varepsilon_{\text{eff,root}}$) divided by the nominal strain range ($\Delta\varepsilon_n$). The difference of the effective notch strain range between the weld toe and root is relatively large in the toe failure specimen, whereas it becomes small in the toe-root specimen. Figure 14 shows the effective notch strain range in terms of the weld leg length ratio between the FL and FLH specimens, in which the incomplete penetration ratio is almost same. The same tendency can be observed in Fig. 13 with respect to the relation between the effective notch strain range of the weld toe and root and failure pattern.

The ratio of the effective notch strain range at the weld root to that at the weld toe ($\Delta\varepsilon_{\text{eff,root}}/\Delta\varepsilon_{\text{eff,toe}}$) was used to indicate the cracking location. The ratios calculated for the specimens are given in Table 7. Additionally, the ratios of the root failure specimens in a previous study [14] are also given in the table. The results reveal that the ratios tended to be less than 1.0 in the toe and toe-root failure specimens. By contrast, the ratio becomes higher than 1.0 in the root failure specimen. Consequently, the effective notch strain range ratio can be used to determine the cracking location.

5 Conclusions

This study carried out the low-cycle fatigue tests using load-carrying cruciform-welded joints with incomplete penetration in order to investigate fatigue strength and failure pattern. The test results revealed that the fatigue strength and failure pattern were affected by the ratio of the incomplete penetration size to the main plate thickness and the ratio of the weld leg length to the main plate thickness. In addition, FE analyses introducing the effective notch concept showed that the effective notch strain range can be used to evaluate the fatigue strength of cruciform joints and that there exists the possibility that the crack initiation point and failure pattern can be predicted by comparing the effective notch strain range between the weld toe and the weld root.

Acknowledgments The authors gratefully acknowledge the support of the Japan Welding Engineering Society and would like to express their sincere gratitude to Dr. Tsuyama at KAWADA INDUSTRIES, Inc. and Mr. Takebuchi at MK ENGINEERING, Inc., for fabricating the specimens.

References

1. Miki C, Hirabayashi Y (2007) Fatigue damage cases due to inappropriate fabrication in steel bridge structures. *Doboku Gakkai Ronbunshuu A*, JSCE 63(3):518–532 (in Japanese)
2. Maddox SJ (1974) Assessing the significance of flaws in welds subject to fatigue. *Welding Research Supplement*:401s–410s
3. Gurney TR (1979) *Fatigue of welded structure*, 2nd edn. Syndics of the Cambridge University Press
4. Frank KH, Fisher JW (1979) Fatigue strength of fillet welded cruciform joints. *Journal of Structural Division*, ASCE 105(ST9): 1727–1740
5. Miki C, Tateishi K, Fan H, Tanaka M (1993) Fatigue strengths of fillet-welded joints containing root discontinuities. *Int J Fatigue* 15(2):133–140
6. Kainuma S, Mori T, Ichimiya M (2001) Evaluation method for fatigue failure modes in load-carrying fillet welded cruciform joints. *Journal of JSCE No.668/I-54*:313–318 (in Japanese)
7. Kainuma S, Mori T (2006) A fatigue strength evaluation method for load-carrying fillet welded cruciform joints. *Int J Fatigue* 28(8): 864–872
8. Kainuma S, Mori T (2008) A study on fatigue crack initiation point of load-carrying fillet welded cruciform joints. *Int J Fatigue* 30(9): 1669–1677
9. Ishii Y, Iida K (1969) Low and intermediate cycle fatigue strength of butt welds containing weld defects. *Journal of JSNDI* 18(10): 443–474
10. Seto A, Masuda T, Machida S, Miki C (1999) Very low cyclic fatigue properties of butt welded joints containing weld defects. *Quarterly Journal of the JWS* 17(1):130–138 (in Japanese)
11. Hanji T, Miki C, Saiprasertkit K (2012) Low and high cycle fatigue behaviour of load-carrying cruciform joints containing incomplete penetration and strength mismatch. *Welding in the World*, IIW 56(5/6):133–146
12. Saiprasertkit K, Hanji T, Miki C (2012) Fatigue strength assessment of load-carrying cruciform joints with material mismatching in low- and high-cycle fatigue regions based on the effective notch concept. *Int J Fatigue* 40:120–128
13. Saiprasertkit K, Hanji T, Miki C (2012) Local strain estimation method for low- and high-cycle fatigue strength evaluation. *Int J Fatigue* 40:1–6
14. Saiprasertkit K, Sasaki E, Miki C (2014) Fatigue crack initiation point of load carrying cruciform joints in low and high cycle fatigue regions. *Int J Fatigue* 59:153–158
15. ASTM (2013) E140: standard hardness conversion tables for metals relationship among Brinell hardness, Vickers hardness, Rockwell hardness, superficial hardness, Knoop hardness, Scleroscope hardness, and Leeb hardness
16. Fricke W (2008) Guideline for the fatigue assessment by notch stress analysis for welded structures, IIW Documentation, XIII-2240-08/XV-1289-08,

Publisher's note Springer Nature remains neutral with regard to jurisdictional claims in published maps and institutional affiliations.